First cosmological results using Type Ia supernovae from the Dark Energy Survey: measurement of the Hubble constant

E. Macaulay [1]★ R. C. Nichol,[1] D. Bacon,[1] D. Brout,[2] T. M. Davis,[3] B. Zhang,[4,5]
B. A. Bassett,[6,7] D. Scolnic,[8] A. Möller,[4,5] C. B. D'Andrea,[2] S. R. Hinton,[3]
R. Kessler,[8,9] A. G. Kim,[10] J. Lasker,[8,9] C. Lidman,[5] M. Sako,[2] M. Smith,[11]
M. Sullivan,[11] T. M. C. Abbott,[12] S. Allam,[13] J. Annis,[13] J. Asorey,[14] S. Avila,[1]
K. Bechtol,[15] D. Brooks,[16] P. Brown,[17] D. L. Burke,[18,19] J. Calcino,[3] A. Carnero
Rosell,[20,21] D. Carollo,[22] M. Carrasco Kind,[23,24] J. Carretero,[25] F. J. Castander,[26,27]
T. Collett,[1] M. Crocce,[26,27] C. E. Cunha,[18] L. N. da Costa,[21,28] C. Davis,[18] J. De
Vicente,[20] H. T. Diehl,[13] P. Doel,[16] A. Drlica-Wagner,[8,13] T. F. Eifler,[29,30] J. Estrada,[13]
A. E. Evrard,[31,32] A. V. Filippenko,[33,34]† D. A. Finley,[13] B. Flaugher,[13] R. J. Foley,[35]
P. Fosalba,[26,27] J. Frieman,[8,13] L. Galbany,[36] J. García-Bellido,[37] E. Gaztanaga,[26,27]
K. Glazebrook,[38] S. González-Gaitán,[39] D. Gruen,[18,19] R. A. Gruendl,[23,24]
J. Gschwend,[21,28] G. Gutierrez,[13] W. G. Hartley,[16,40] D. L. Hollowood,[35]
K. Honscheid,[41,42] J. K. Hoormann,[3] B. Hoyle,[43,44] D. Huterer,[32] B. Jain,[2] D.
J. James,[45] T. Jeltema,[35] E. Kasai,[7,46] E. Krause,[29] K. Kuehn,[47] N. Kuropatkin,[13]
O. Lahav,[16] G. F. Lewis,[48] T. S. Li,[8,13] M. Lima,[21,49] H. Lin,[13] M. A. G. Maia,[21,28] J.
L. Marshall,[17] P. Martini,[41,50] R. Miquel,[25,51] P. Nugent,[10] A. Palmese,[13] Y.-C. Pan,[52,53]
A. A. Plazas,[30] A. K. Romer,[54] A. Roodman,[18,19] E. Sanchez,[20] V. Scarpine,[13]
R. Schindler,[19] M. Schubnell,[32] S. Serrano,[26,27] I. Sevilla-Noarbe,[20] R. Sharp,[5]
M. Soares-Santos,[55] F. Sobreira,[21,56] N. E. Sommer,[4,5] E. Suchyta,[57] E. Swann,[1] M. E.
C. Swanson,[24] G. Tarle,[32] D. Thomas,[1] R. C. Thomas,[10] B. E. Tucker,[4,5] S. A. Uddin,[58]
V. Vikram,[59] A. R. Walker,[12] and P. Wiseman[11] (DES Collaboration)

Affiliations are listed at the end of the paper

Accepted 2019 April 3. Received 2019 April 2; in original form 2018 November 8

ABSTRACT

We present an improved measurement of the Hubble constant (H_0) using the 'inverse distance ladder' method, which adds the information from 207 Type Ia supernovae (SNe Ia) from the Dark Energy Survey (DES) at redshift $0.018 < z < 0.85$ to existing distance measurements of 122 low-redshift ($z < 0.07$) SNe Ia (Low-z) and measurements of Baryon Acoustic Oscillations (BAOs). Whereas traditional measurements of H_0 with SNe Ia use a distance ladder of parallax and Cepheid variable stars, the inverse distance ladder relies on absolute distance measurements from the BAOs to calibrate the intrinsic magnitude of the SNe Ia. We find $H_0 = 67.8 \pm 1.3$ km s^{-1} Mpc^{-1} (statistical and systematic uncertainties, 68 per cent confidence). Our measurement makes minimal assumptions about the underlying cosmological model, and our analysis was blinded to reduce confirmation bias. We examine possible systematic uncertainties and all are

★ E-mail: edward.macaulay@port.ac.uk
† Miller Senior Fellow

below the statistical uncertainties. Our H_0 value is consistent with estimates derived from the Cosmic Microwave Background assuming a ΛCDM universe.

1 INTRODUCTION

The precise value of the Hubble constant (H_0) has again become one of the most debated topics in cosmology (see Freedman 2017). This debate has been fuelled by the apparent disagreement between local, direct measurements of H_0, primarily Riess et al. (2016) who find $H_0 = 73.24 \pm 1.74$ km s^{-1} Mpc^{-1}, and estimates derived from the Cosmic Microwave Background (CMB) which give $H_0 = 67.4 \pm 0.5$ km s^{-1} Mpc^{-1} (Planck Collaboration 2018), assuming a ΛCDM universe. This discrepancy has increased to 3.7σ with new parallax measurements to Cepheid variable stars by Riess et al. (2018) giving $H_0 = 73.48 \pm 1.66$ km s^{-1} Mpc^{-1}.

This tension between the local measurements of the Hubble constant and the Planck + ΛCDM expectation may be due to unknown systematic uncertainties in the various observations, flaws in the theoretical assumptions, and/or underestimation of the uncertainties on the measurements of H_0 (see e.g. discussion in Zhang et al. 2017b).

Sample or cosmic variance has been proposed as a potential systematic effect for direct measurements of H_0. Cepheid variable stars can only be observed in the nearest galaxies, and the number of such galaxies that also have a well-determined SN Ia with which to calibrate the SN Ia luminosity zero-point is small. Thus these measurements only probe a small cosmological volume with a low number of galaxies for cross-calibration. However, Wu & Huterer (2017) used *N*-body simulations to evaluate the sample variance, and found that it contributes a dispersion of 0.31 km s^{-1} Mpc^{-1} to the local measurements of H_0, which is too small to account for the discrepancy with Planck.

The discrepancy in H_0 may alternatively be due to physics beyond the ΛCDM model (Bernal, Verde & Riess 2016; Di Valentino, Melchiorri & Silk 2016; Riess et al. 2016; Di Valentino, Linder & Melchiorri 2018). A negative curvature ($\Omega_k < 0$) could account for the discrepancy, which would have implications for models of cosmic inflation (de Putter, Linder & Mishra 2014; Grandis et al. 2016; Farooq et al. 2017). Modifications to gravity could cause a larger acceleration than expected in ΛCDM (Pourtsidou & Tram 2016; Di Valentino, Melchiorri & Mena 2017; Zhao et al. 2017). Alternatively, an additional relativistic species at the CMB epoch could account for the tension (Moresco et al. 2012; Vagnozzi et al. 2017). We note however that explanations for the H_0 tension involving modified gravity, or an extra relativistic species, would increase tensions in measurements of σ_8 (the amplitude of the matter power spectrum) and expectations from Planck + ΛCDM (e.g. Macaulay, Wehus & Eriksen 2013; Yang & Xu 2014; Costa et al. 2017; Joudaki et al. 2017).

This tension has motivated the development of new, independent ways to measure H_0. For example, Birrer et al. (2019) find $H_0 = 72.5^{+2.1}_{-2.3}$ km s^{-1} Mpc^{-1} from measurements of time delays from strongly lensed quasars, and Guidorzi et al. (2017) find $H_0 = 75.5^{+11.6}_{-9.6}$ km s^{-1} Mpc^{-1} by using the gravitational wave event GW170817 as a standard siren.

In this paper, we present a new measurement of H_0 using spectroscopically confirmed SNe Ia from the Dark Energy Survey (see Flaugher et al. 2015; DES Collaboration 2018a, for details). Since SNe Ia are relative, not absolute, distance indicators, their intrinsic magnitude must be calibrated using an absolute distance

measurement. This is the motivation behind the conventional distance ladder approach of calibrating local SNe Ia using Cepheid variable stars and parallax. The approach we take is to calibrate the intrinsic magnitude of SNe Ia against the absolute distance measurements from the Baryon Acoustic Oscillations (BAOs) at $z > 0.1$ (assuming the sound horizon from the CMB). We then use the calibrated SN Ia distances to trace the expansion history of the Universe back to $z = 0$ to determine H_0.

We note that although BAO measurements alone could derive a value for H_0 (see e.g. Fig. 1), it would rely on the assumption of a cosmological model to extrapolate the BAO measurements to $z = 0$ (see e.g. DES Collaboration 2018b). By using calibrated SNe Ia across a range of redshifts, we can determine H_0 more directly without assuming a specific cosmological model such as ΛCDM.

H_0 was first measured using this 'inverse distance ladder' technique by Aubourg et al. (2015), who found $H_0 = 67.3 \pm 1.1$ km s^{-1} Mpc^{-1} with SNe Ia from the Joint Light-Curve Analysis (JLA; Betoule et al. 2014) and BAO measurements from the Baryon Oscillation Spectroscopic Survey (BOSS) Data Release Eleven (DR11). This result was updated with BOSS DR12 in Alam et al. (2017), finding $H_0 = 67.3 \pm 1.0$ km s^{-1} Mpc^{-1}.

In this paper, we use 207 new, spectroscopically confirmed SNe Ia from the DES Supernova Program (DES-SN3YR) to measure H_0 with this inverse distance ladder technique. While this sample contains fewer supernovae than JLA, the DES-SN3YR sample has the key advantage of spanning the entire redshift range of the available galaxy BAO measurements (e.g. $z_{\rm eff} = 0.112$–0.61) in a single survey. This is not true of other inverse distance ladder measurements which rely on the JLA sample, because different SN surveys must be combined in order to cover this redshift range (e.g. the SDSS SN sample at $z \simeq 0.1$, SNLS at $z \simeq 0.6$).

We describe the data and method used for our analysis in Section 2, and our results in Section 3. We conclude in Section 4.

2 METHODOLOGY AND DATA

We use a similar methodology as Aubourg et al. (2015), using BAO distance measurements to calibrate the SNe Ia. This breaks the well-known degeneracy between the SNe Ia peak absolute magnitude and H_0. While BAO data alone can constrain H_0, these measurements typically assume a specific cosmological model (e.g. a cosmological constant as in DES Collaboration 2018b), since the BAO measurements do not have sufficient redshift coverage to determine $H(z)$ on their own (Fig. 1 illustrates this point). By combining BAO and SNe Ia, we can relax the assumption of a specific cosmological model when determining H_0.

However, we do still require some model for the redshift–distance relationship to extrapolate these data to $z = 0$. For this work, we adopt a cosmographical approach for the redshift–distance relationship, which is a smooth Taylor expansion about redshift, that makes minimal assumptions about the underlying cosmological model (Muthukrishna & Parkinson 2016; Zhang, Li & Xia 2017a; Feeney et al. 2019). We use equations (6), (7) and (8) in Zhang et al. (2017a) to determine the luminosity distance $D_{\rm L}(z)$ and Hubble parameter $H(z)$ as a function of redshift. $D_{\rm L}(z)$ is given by

$$D_{\rm L}(z) = z + C_1 z^2 + C_2 z^3 + C_3 z^4 + C_4 z^5 + ..., \qquad (1)$$
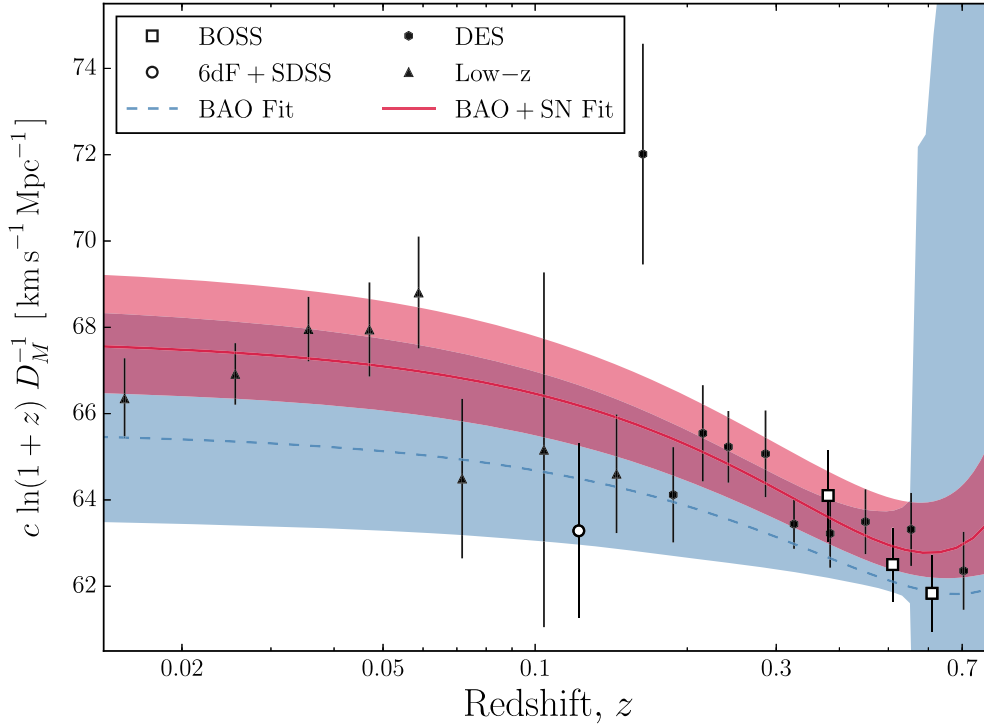
Figure 1. Here we illustrate the inverse distance ladder method. The white data points are the BAO distance measurements, and the black data points are the SNe Ia data. The DES-SN3YR sample comprises the higher redshift DES SNe (illustrated with hexagonal points), and the Low-z SNe (illustrated with triangular points). The red line shows our best-fitting cosmographical model, and the shaded region is the 68 per cent confidence region. The blue dashed line and shaded region illustrates the equivalent constraints from just the BAO data, without any supernovae. The blue, BAO-only region is very large at $z > 0.7$ because we fit only for r_s, and not the absolute distance scale at the CMB.

where

$$C_1 = \frac{1}{2}(1 - q_0), \tag{2}$$

$$C_2 = -\frac{1}{6}(1 - q_0 - 3q_0^2 + j_0), \tag{3}$$

$$C_3 = \frac{1}{24}(2 - 2q_0 - 15q_0^2 + 5j_0 + 10q_0 j_0 + s_0), \tag{4}$$

and

$$C_4 = \frac{1}{120}(-6 + 6q_0 + 81q_0^2 + 165q_0^3 + 105q_0^4 + 10j_0^2 - 27j_0 \\ - 110q_0 j_0 - 105q_0^2 j_0 - 15q_0 s_0 - 11s_0 - l_0). \tag{5}$$

$H(z)$ is given by

$$H(z) = H_0[1 + (1 + q_0)z + \frac{1}{2}(-q_0^2 + j_0)z^2 \\ + \frac{1}{6}(3q_0^2 + 3q_0^3 - 4q_0 j_0 - 3j_0 - s_0)z^3 \\ + \frac{1}{24}(-12q_0^2 - 24q_0^3 - 15q_0^4 + 32q_0 j_0 + 25q_0^2 j_0 \\ + 7q_0 s_0 + 12j_0 - 4j_0^2 + 8s_0 + l_0)z^4] + ... \tag{6}$$

We find that including the lerk (l_0) parameter (z^5) in our cosmographic model increases the Bayesian Information Criterion from 40.4 to 44.1, which indicates that including this additional parameter is not warranted by the data. The fitting parameters in this Taylor expansion are then H_0 (Hubble constant), q_0 (deceleration), j_0 (jerk), and s_0 (snap). This is consistent with Gómez-Valent & Amendola

(2018) who found that fourth-order polynomials and above made minimal improvement to the Bayesian and Akaike information criteria when fitting a larger set of data including both SNe Ia and other cosmological data sets. They also noted that such higher order polynomials had minimal effect on the value of H_0 they determined. We assume uniform priors on these cosmographical parameters and therefore, our results are relatively insensitive to the details of the assumed underlying late-time redshift–distance relationship.

Throughout, we must assume the validity of the cosmic distance–duality relation; that the luminosity distance $D_L(z)$ is related to the angular diameter distance $D_A(z)$ by $D_L(z) = D_A(z)(1 + z)^2$. This well-known relationship in cosmology is applicable to general metric theories of gravity in which photons are conserved and travel on null geodesics (see e.g. Bassett & Kunz 2004).

To determine H_0, we perform a combined analysis of SNe Ia and BAO with a Gaussian prior on r_s (the sound horizon at recombination) based on CMB data. All these data are required and complementary, and assumed to be independent. The individual likelihood functions are assumed to be Gaussian and given by

$$\ln \mathcal{L}_x = \Delta_x^T \mathsf{C}^{-1} \Delta_x, \tag{7}$$

where x above is either SNe Ia or BAO data. C is the data covariance matrix for either data set, and Δ_x is the difference vector between the data sets and their corresponding values in the cosmographical model.

These likelihood functions are then combined to give

$$\ln \mathcal{L}(\Theta, M_B^1, r_s) = \ln \mathcal{L}_{SN}(\Theta, M_B^1) + \ln \mathcal{L}_{BAO}(\Theta, r_s) + \ln \mathcal{L}_{r_s}(r_s), \tag{8}$$

where $\Theta = [H_0, q_0, j_0, s_0]$ is a common set of cosmographic parameters and M_B^1 is the SNe Ia absolute magnitude at peak (see Section 2.2).

2.1 Baryon acoustic oscillations

The scale of the BAO is a well-established cosmological standard ruler (e.g. Blake & Glazebrook 2003; Seo & Eisenstein 2003; Eisenstein et al. 2005; Blake et al. 2011; Busca et al. 2013; Anderson et al. 2014; Alam et al. 2017). With the physical scale set by the sound horizon at recombination (r_s), BAOs provide absolute distance measurements over a range of redshifts. In order to measure the BAO signal from galaxy redshift surveys, a fiducial cosmology must be assumed in order to convert the observed angles and redshifts into distances.

We emphasize that this does not imply that a BAO measurement is limited to a consistency test of that assumed fiducial cosmology, since most BAO analyses typically fit for α^{BAO}, a dimensionless parameter measuring the ratio of the observed BAO scale to the scale expected in the fiducial cosmology.

An isotropic BAO analysis, where the BAO signal is measured from pairs of galaxies averaged over all angles, is sensitive to the volume averaged distance (e.g. D_V, see Aubourg et al. 2015). We can relate the expected $D_V(\Theta, z)$ to the observed α^{BAO} and the fiducial BAO values by

$$\frac{D_V(\Theta, z)}{r_s} = \alpha^{BAO} \frac{D_V^{fid}(z)}{r_s^{fid}}, \tag{9}$$

where

$$D_V(\Theta, z) = [z D_H(\Theta, z) D_M^2(\Theta, z)]^{1/3}. \tag{10}$$

$D_H(\Theta, z)$ is the Hubble distance, given by

$$D_H(\Theta, z) = \frac{c}{H(\Theta, z)}, \tag{11}$$

and $D_M(\Theta, z)$ is the comoving angular diameter distance.

In our likelihood analysis, we use the observed $D_V(z_{eff} = 0.122) = 539 \pm 17(r_s/r_s^{fid})$ Mpc (68 per cent confidence) taken from Carter et al. (2018), based on a reanalysis of the 6-deg Field Galaxy Survey (Beutler et al. 2011) and Sloan Digital Sky Survey Main Galaxy Sample (Ross et al. 2015).

At higher redshift, we use the 'Consensus' BOSS DR12 data set from Alam et al. (2017) which provides a two-dimensional description of the clustering, dividing the separation between pairs of galaxies into components across and along the line of sight, now summarizing the clustering with two parameters of $\alpha_\perp^{BAO}$ and $\alpha_\parallel^{BAO}$, respectively. Their expected values can now be related to their observed values by

$$\frac{D_M(\Theta, z)}{r_s} = \alpha_\perp^{BAO} \frac{D_M^{fid}(z)}{r_s^{fid}}, \tag{12}$$

and

$$\frac{D_H(\Theta, z)}{r_s} = \alpha_\parallel^{BAO} \frac{D_H^{fid}(z)}{r_s^{fid}}. \tag{13}$$

The BOSS DR12 data set consists of measurements of $D_M(z)$ and $H(z)$ at three effective redshifts of $z_{eff} = [0.38, 0.51, 0.61]$ (six measurements in total). The covariance matrix for these six measurements includes the correlation between $D_M(z)$ and $H(z)$ at each z_{eff}, and the correlation between these six measurements in different redshift bins.

In equation (7), $\ln \mathcal{L}_{BAO}(\Theta, r_s)$ is then the combined likelihood of the two BAO data sets from Carter et al. (2018) and BOSS

DR12. This likelihood requires knowledge of the sound horizon at recombination (r_s), which depends on the sound speed at these earlier epochs and thus the baryon density (ω_b) and the total matter density (ω_{cb}) in the early universe (see equation 16 of Aubourg et al. 2015).

In our analysis, we adopt a Gaussian prior on r_s of 147.05 ± 0.30 Mpc (68 per cent confidence) taken from the Planck 2018 analysis (TT,TE,EE + lowE result in Table 2). By using the value of r_s derived from only the TT,TE,EE + lowE Planck data, we minimize our sensitivity to physics of the late-time universe. Of these effects, CMB lensing is the most significant, although Feeney et al. (2019) note that even including CMB lensing changes their value of H_0 by less than the statistical uncertainty on this measurement.

We explore the sensitivity of our results to this prior in Section 4, but note that the Planck measurement of r_s comes from their measurement of the baryon and total matter densities, which in turn are only related to the heights of the acoustic peaks in the CMB power spectrum and not on their angular locations. Therefore, any dependencies introduced because of this Planck prior are based only on our correct understanding of plasma physics in the pre-recombination epoch, rather than assumptions about curvature and late-time dark energy, which are negligible in the early Universe for many cosmological models.

2.2 Type Ia supernovae

Type Ia supernovae are cosmological standard candles (e.g. Riess et al. 1998; Perlmutter et al. 1999; Hicken et al. 2009; Kessler et al. 2009; Sullivan et al. 2010). In this analysis, we use the DES-SN3YR sample of 207 new, spectroscopically confirmed SNe Ia from the first three years of DES, which are supplemented by 122 SNe Ia from the CfA3 (Hicken et al. 2009), CfA4 (Hicken et al. 2012), and CSP Low-z sample (Hamuy et al. 2006; Contreras et al. 2010; Folatelli et al. 2010; Stritzinger et al. 2011; Krisciunas et al. 2017) ($z < 0.09$) described in part in Scolnic et al. (2018).

The details of the DES-SN3YR sample are provided in a series of papers as part of the overall DES-SN 3 year cosmology paper by DES Collaboration (2018c). D'Andrea et al. (2018) describes the spectroscopic follow-up observations, Brout et al. (2019b) outlines the supernova scene model photometry, Lasker et al. (2019) details the DES photometric corrections, Kessler et al. (2019) presents the survey simulations and selection function. Brout et al. (2019a) presents validations of the sample, systematic uncertainties, light-curve fits, and distance measurements.

Our analysis uses the distances and covariance matrices derived in Brout et al. (2019a) with the 'BBC' (BEAMS with Bias Correction) method (Kessler & Scolnic 2017). The distances have been binned in 18 redshift bins (originally 20 bins, but with 2 empty bins).

The distance modulus, μ, for these supernovae is given by

$$\mu(\Theta, z) = 25 + 5 \log_{10} (D_L(\Theta, z)), \tag{14}$$

where $D_L(\Theta, z)$ is the luminosity distance. We relate μ to the observed SALT2 (Guy et al. 2007) light-curve parameters by

$$\mu = m_B - M_B^1 + \alpha X_1 - \beta C + \Delta m_{host} + \Delta B, \tag{15}$$

where m_B is the observed B-band peak magnitude, M_B^1 is the absolute magnitude of the SNe Ia, X_1 is the stretch parameter of the light curve, and C is the colour parameter. α and β are free parameters which are fitted for when calculating the distances. Also, Δm_{host} is a correction applied for host galaxy masses of $M_{stellar} > 10^{10} M_\odot$ (see also Sullivan et al. 2010; Kelly et al. 2010; Lampeitl

et al. 2010b). The stellar mass measurements for the host galaxies were obtained from fits to the DES SV galaxy photometry with the galaxy evolution modelling code ZPEG (Le Borgne & Rocca-Volmerange 2002; see Smith et al. 2019, in preparation for details). ΔB is the expected μ-correction due to the survey selection function for both the DES-SN3YR sample as discussed in detail in Brout et al. (2019a).

3 RESULTS

We use EMCEE (Foreman-Mackey et al. 2013) as our Markov chain Monte Carlo sampler to determine the joint likelihood of our parameters (H_0, q_0, j_0, s_0, r_s, M_B^1) in equation (8). These joint likelihoods are shown in Fig. 2 along with the marginalized likelihood functions for all the fitted parameters.

We blinded our analysis throughout the analysis to reduce confirmation bias (e.g. Croft & Dailey 2015). This blinding has been achieved by preparing and testing all our codes and plots using either simulated DES-SN3YR samples (see Appendix for details) or the existing JLA sample from Betoule et al. (2014). We only replaced these testing data files with the genuine DES-SN3YR sample before submission to the DES collaboration for internal collaboration review. Before unblinding, we reviewed the results with unknown random offsets added to the chains, so that the shape of the likelihoods and the uncertainties could be assessed without influence from the maximum likelihood values of the chains. After unblinding, some minor updates to the SN-data covariance matrix were introduced, including the use of two different intrinsic dispersion values for the DES and Low-z samples. Updating our results after unblinding did not significantly change our results or conclusions.

In Table 1 we summarize our H_0 measurements with different supernovae surveys. We note that the χ^2/ d.o.f increases for all of the combined fits with SNe Ia data. This is consistent with the higher H_0 values in the combined fits than the BAO-only case, and suggests that the best-fitting cosmographic model favours increased expansion at lower redshifts than the BAO surveys.

We note that our cosmographical method can reproduce the H_0 measurement from Alam et al. (2017). Using the same data set (namely, JLA supernovae, BOSS DR12 BAOs, and the older BAO measurements from Beutler et al. 2011 and Ross et al. 2015), we find $H_0 = 67.1 \pm 1.3$ km s^{-1} Mpc^{-1}. We do not use the BAO measurements from Beutler et al. (2011) and Ross et al. (2015) elsewhere, since they are superseded by the combined analysis of Carter et al. (2018).

We find a larger uncertainty than Alam et al. (2017), which may be due to the more general model we are using for the redshift–distance relation. Instead of the cosmographic model used here, Alam et al. (2017) use a 'PolyCDM' cosmological model, which is the ΛCDM model, plus two additional arbitrary density components, Ω_1 and Ω_2, which scale with linear and quadratic order with redshift, in order to allow for deviations from ΛCDM.

We find that our best-fitting parameters are consistent with previous analyses. For example, we find $M_B^1 = -19.12 \pm 0.03$ mag (68 per cent confidence) which is consistent with the value from Aubourg et al. (2015) of $M_B^1 = -19.14 \pm 0.042$ mag. Moreover, Fig. 2 illustrates that, as expected, SNe Ia alone are unable to constrain this parameter, given the strong correlation with H_0 (also seen in the figure).

The cosmographical parameters are constrained by both BAO and SNe Ia. The deceleration parameter shows a significant, negative value of $q_0 = -0.37 \pm 0.15$ (68 per cent confidence), even after marginalizing over other parameters. This value is consistent with other q_0 measurements in the literature (e.g. Lampeitl et al. 2010a found $q_0 = -0.34 \pm 0.18$ from just the SDSS SN sample) but less negative than expected for a Λ–dominated cosmology (e.g. $q_0 = -0.55$ from Capozziello, Cardone & Salzano 2008). Other cosmographical parameters (j_0, s_0) are best constrained by the SNe Ia data (green contours), and consistent with zero and expectations from ΛCDM given our uncertainties.

We find $H_0 = 67.8 \pm 1.3$ km s^{-1} Mpc^{-1} (68 per cent confidence), with a reduced χ^2 of 1.16. This measurement is consistent with the Planck value of $H_0 = 67.4 \pm 0.5$ km s^{-1} Mpc^{-1}, but inconsistent at 2.5 σ to the recent Riess et al. (2018) local distance ladder measurement.

We make no further comment on this tension as there is already significant literature (see e.g. Freedman 2017) on the possible systematic uncertainties involved in all measurements and/or interesting new physics that could be responsible. However, we emphasize the independence of this result to that of Riess et al. (2018): although both measurements rely on SNe Ia, the Cepheid-calibrated distance ladder method of Riess et al. (2018) is very different to the BAO-calibrated inverse distance ladder method used here. Our measurement is in excellent agreement with previous inverse distance ladder measurements, e.g. Alam et al. (2017) who used the JLA sample, as well more recent measurements using the Pantheon SN sample (Feeney et al. 2019; Lemos et al. 2019).

In Fig. 1, we provide an illustration of the inverse distance ladder method and the importance of both BAO and SNe Ia data for deriving the best constraint on H_0. The SNe Ia data is the DES-SN3YR sample (18 redshift bins) and the SN and BAO uncertainties are the square roots of the corresponding diagonal elements of their covariance matrices. We also show our best-fitting cosmographical model (with associated 68 per cent confidence band in red) as well as the best-fitting BAO-only cosmographical model and uncertainty band (in blue).

4 DISCUSSION AND CONCLUSIONS

Although our H_0 value is in excellent agreement with Planck Collaboration (2018), we emphasize that the use of an r_s prior from Planck does not imply that our measured value of H_0 will inevitably agree with the value of H_0 derived from Planck cosmological parameters assuming a ΛCDM cosmology.

The value of r_s is informed by only the baryon and matter densities at $z = 1090$; there are many viable cosmological models which are consistent with only these two quantities (or, in other words, this value of r_s) that have wildly different values of the Hubble constant at $z = 0$.

Indeed, our BAO-only value of $H_0 = 65.7 \pm 2.4$ km s^{-1} Mpc^{-1} is lower than the Planck-derived value. The BAO data only directly constrain the expansion down to $z \sim 0.12$. Extrapolating to $z = 0$ thus leads to larger uncertainties from the BAO-only than from the BAO + SNe Ia because the SNe Ia probe down to $z = 0.015$. The consistency between our measurement and the derived Planck value is instead a reflection of the consistency between the cosmology traced by the SN and BAO data and the model used to derive the Planck value.

4.1 Systematic uncertainty budget

We now consider the possible systematic uncertainties that may affect our result. As in Brout et al. (2019a), we consider contributions to the total uncertainty from many contributions of systematic
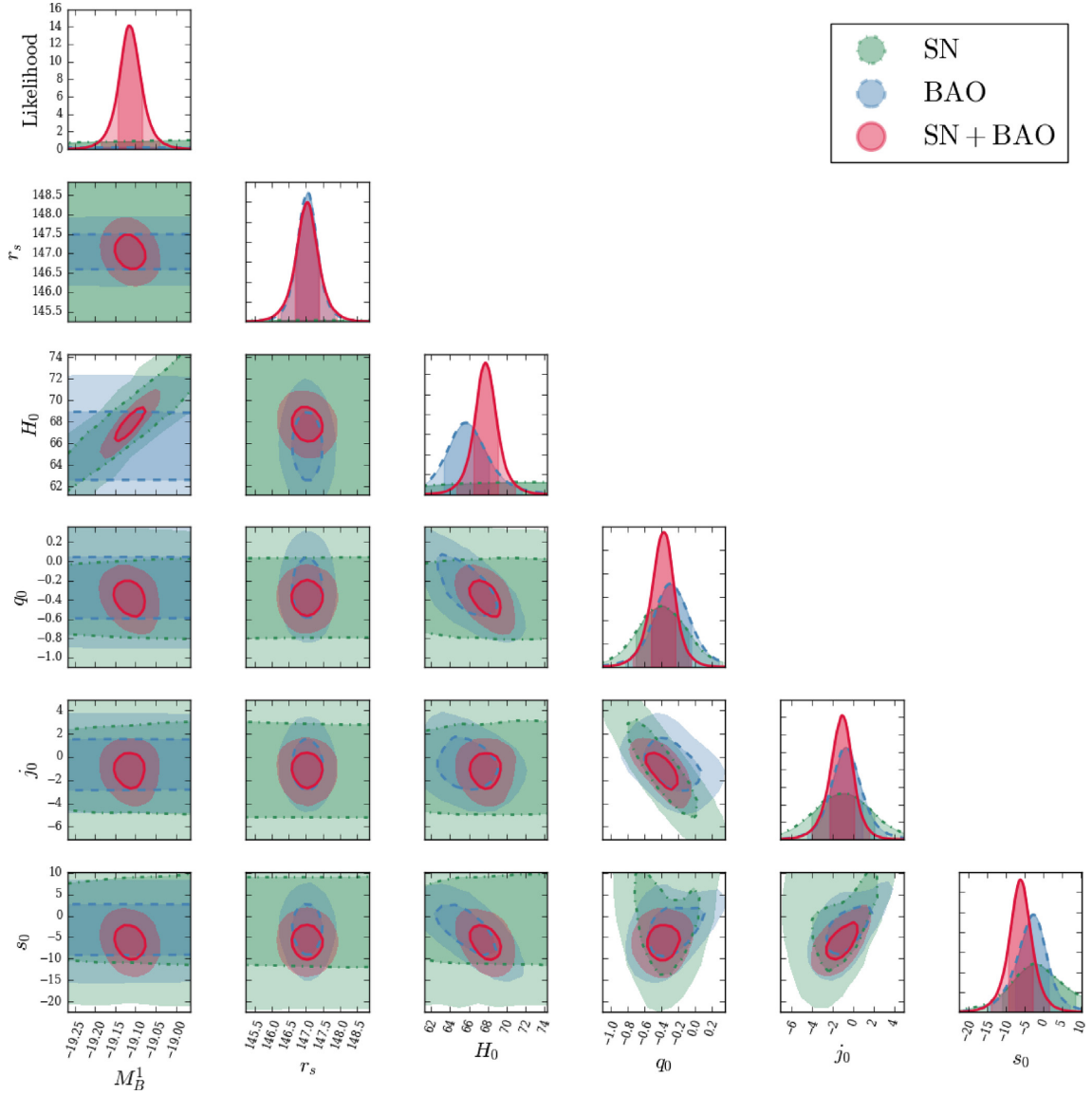
Figure 2. The parameter constraints on our model from supernovae (green, dot–dashed lines), BAO (blue, dashed lines), and both data sets combined (red, solid lines). We can see that the supernovae constraints on H_0 and M_B^1 are degenerate, and r_s is entirely unconstrained, although the cosmographic parameters of q_0, j_0, and s_0 (which affect the shape of the Hubble diagram) are well constrained. We can also see that the BAO-only constraint on H_0 is correlated with all of the cosmographic parameters. The power of the combined fit is driven by the degree of orthogonality of the individual constraints, particularly in the H_0–M_B^1 plane. .

Table 1. A summary of our H_0 measurements. We fit all the data sets with six free parameters (except for the BAO-only case, with five free parameters, since we do not fit for M_B).

Data	H_0 (km s^{-1} Mpc^{-1})	d.o.f.	χ^2/d.o.f.	p-value
BAO Only	65.7 ± 2.4	2	0.75	0.47
+ JLA	67.1 ± 1.3	33	1.28	0.13
+ Low-z	66.1 ± 2.6	10	0.94	0.49
+ DES	66.9 ± 1.9	12	1.28	0.22
+DES + Low-z	67.8 ± 1.3	20	1.16	0.28

uncertainty. To quantify the effect of each systematic uncertainty, we first repeat our analysis with only the statistical uncertainties included in the supernova data covariance matrix, to find the statistical-only uncertainty on H_0, σ_{stat}. We then repeat this analysis for each of the sources of systematic uncertainty, including each contribution of systematic uncertainty in the supernova covariance matrix, to find the combined uncertainty due to statistics and the particular systematic, $\sigma_{\text{stat + sys}}$. We then define the systematic only uncertainty as

$$\sigma_{\text{sys}} = \sqrt{\sigma_{\text{stat+sys}}^2 - \sigma_{\text{stat}}^2}. \tag{16}$$

We consider systematic uncertainties due to DES and Low-z calibration, SALT fitting, Supercal calibration (Scolnic et al. 2015), the intrinsic scatter model, colour parameter parent populations,

Table 2. The contributions of systematic uncertainties on our H_0 measurement. For each term we quantify the shift in the value of H_0, the value of the systematic uncertainty, and the fraction of the uncertainty compared to the statistical uncertainty. The individual uncertainties will not necessarily sum in quadrature to the total uncertainty, due to different redshift weightings and correlations in each term.

Description	H_0 shift	σ_{syst}	$\sigma_{syst} / \sigma_{stat}$
Total Stat.	0.000	1.048	1.00
Total Sys.	0.162	0.760	0.72
ALL Calibration	-0.078	0.375	0.36
DES Cal.	-0.016	0.276	0.26
Low-z Cal	-0.026	0.254	0.24
SALT	0.053	0.217	0.21
ALL Other	0.004	0.661	0.63
Intrinsic Scatter	0.129	0.330	0.31
$z + 0.00004$	0.036	0.083	0.08
c, x_1 Parent Pop.	-0.031	0.249	0.24
Low-z Vol. Lim.	-0.081	0.124	0.12
Flux Err.	-0.004	0.179	0.17
Spec. Eff	-0.091	0.125	0.12
Ref. Cosmo.	-0.065	0.134	0.13
Low-z 3σ Cut	0.498	0.193	0.18
Sys. Parent	0.370	0.222	0.21
PS1 Coherent Shift	0.064	0.246	0.23
$2\sigma_{int}$	-0.068	0.231	0.22

volume limits, peculiar velocities, flux uncertainty, spectroscopic efficiency, the use of reference cosmology in validation simulations, the Low-z sample 3σ outlier cut, the parent population uncertainty, PS1 Coherent Shift, and the use of two different values of the intrinsic dispersion for the DES and Low-z samples (Brout et al. 2019a). For each of these systematics, in Table 2 we quote the shift in the H_0 value, and also the fractional contribution of the systematic compared to the statistical uncertainty.

We find that the total systematic uncertainty from each of these contributions is 72 per cent of the statistical uncertainty in our measurement; variations below the statistical error are still significant when comparing analysis of the same data. We note that the various individual systematic uncertainties will not necessarily add in quadrature to the total systematic uncertainty, since each systematic introduces a different weighting of the redshift bins.

In Fig. 3, we illustrate the effect of the Low-z sample 3σ outlier cut, the parent population uncertainty, a shift in the absolute wavelength calibration of DES (PS1 Coherent Shift), and the $2\sigma_{int}$ systematic uncertainties. In the upper panel, we illustrate the effect on the observed distances, μ, relative to the statistical-only distances. In the lower panel, we illustrate the corresponding shift in H_0 (again, relative to the statistical-only result).

4.2 BAO calibration

One uncertainty in our analysis is our assumed prior on the sound horizon, based on the Planck CMB measurement. The measurement of r_s is very similar between Planck 2013, 2015, and 2018, and changing between the measurements has a negligible effect on our results. Moreover, Addison et al. (2018) and Lemos et al. (2019) showed that the H_0 tension was still present using non-Planck CMB data for r_s (e.g. WMAP + SPT) or measurements of the primordial deuterium abundance from damped Lyman-α systems to constrain the baryon density, and thus sound horizon, independent of any measurement of the CMB power spectrum.

That said, the existence of 'dark radiation', or an additional relativistic species in the pre-recombination era, could affect the sound horizon. The most obvious candidate would be massive neutrinos, but constraints on such particles are becoming increasingly tight from a combination of the CMB with measurements of the large-scale structure. For example, Yèche et al. (2017) provide a constraint on the sum of the neutrino masses of $\sum m_\mu < 0.8$ eV (95 per cent confidence) with just data from the Lyman-α forest (LyAF). This constraint improves to $\sum m_\mu < 0.14$ eV (95 per cent confidence) when combined with the CMB power spectrum, although adding in the recent DES Y1 clustering analysis (DES Collaboration 2018b) relaxes these constraints to $\sum m_\mu < 0.29$ eV.

Verde et al. (2017) calculated the effect on r_s due to all remaining observationally allowed contributions of dark radiation, and found $r_s = 150 \pm 5$ Mpc. We therefore test our sensitivity to the possibility of early dark radiation by repeating our analysis with this wider prior on r_s. Our results are shown in Fig. 4, and we find $H_0 = 66.32 \pm 2.9$ km s^{-1}Mpc^{-1} (compared to $H_0 = 67.8 \pm 1.3$ km s^{-1} Mpc^{-1} based on our original prior on r_s). As expected, this wider prior increases the uncertainty on H_0, making it more consistent with the value from Riess et al. (2018). We do not include this uncertainty in our uncertainty budget, since the evidence for early dark radiation is not well established, but provide the value for comparison.

As a final test of the sound horizon, we remove any prior on the sound horizon and fit for r_s as a free parameter. Even without any prior on the value of r_s, we are able to place some constraints on r_s (and, correspondingly, H_0) with the minimal assumption that r_s is the same for each of the BAO measurements.

While this assumption would be insufficient in the case of a single (volume averaged) BAO measurement, having multiple BAO measurements at different redshift ranges will – in principle – determine r_s (modulo any uncertainty in the cosmographic parameters). Moreover, in the case of 2D BAO measurements, the consistency of r_s in the parallel and perpendicular measurements further constrains r_s with the Alcock–Paczynski effect. In other words, the value of r_s is – in principle – overdetermined, up to the uncertainties in the cosmographic parameters (which are themselves constrained by the BAO measurements, and also independently by the SN data).

With no prior on r_s, we find $r_s = 145.2 \pm 18.5$ Mpc, which is close to the Planck value, although with a much greater uncertainty, which reduces our sensitivity to H_0, leading to a value of $H_0 = 68.9 \pm 8.9$ km s^{-1}Mpc^{-1}. This test illustrates the importance of knowing the absolute scale of the sound horizon, while also indicating that future BAO measurements from galaxy redshift surveys (e.g. Euclid and DESI) should help constrain this parameter independent of the CMB and thus remove any reliance on early universe plasma physics.

One possible concern is the assumption of a fiducial cosmology in converting the galaxy angular positions and redshifts observed in a galaxy redshift survey (such as BOSS) into the power spectrum of galaxy clustering where the BAO signal is determined. As stated in Section 2.1, this issue is addressed by assuming a scaling law (equation 13) which 'dilates' the distance being tested to the fiducial cosmology used to calculate the galaxy power spectrum. The applicability of such scaling was first studied in detail by Padmanabhan & White (2008) who showed, using N-body simulations, a systematic uncertainty of only $\simeq 1$ per cent on α^{BAO} over a wide range of α^{BAO} values, or more importantly, over a wide range of alternative cosmologies.

It is also worth stressing that the BAO signal is estimated in a series of narrow redshift bins, thus allowing for uncertainties be-
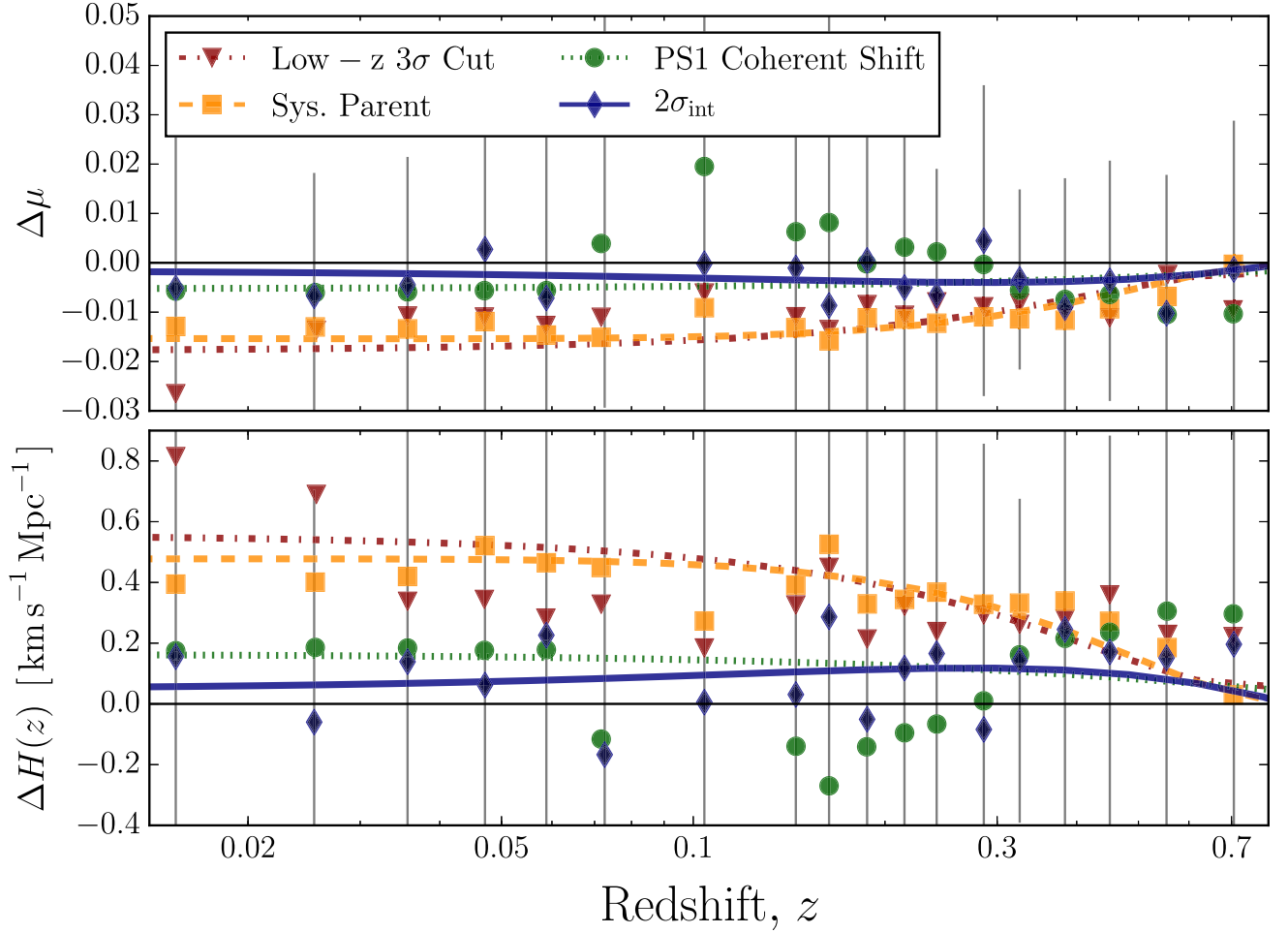
Figure 3. Illustrating the effect of systematic uncertainties. In the upper panel we plot the change in distance modulus, $\Delta\mu$. The supernova data are shown with points, and the best-fitting models are shown with lines. For each systematic, we plot the residual compared to the best-fitting model and data with statistical only uncertainties. In the lower panel, we plot the inferred $H(z)$ residual, again subtracting the statistical-only result. The light-grey vertical lines are the 68 per cent confidence error bars on the data (which we have plotted for only the PS1 Coherent Shift systematic, for clarity). The systematics are described in Section 4.1.

tween the assumed and fiducial cosmology to be minimized across any single redshift shell (assuming cosmologies with a smooth redshift–distance relationship close to ΛCDM). The effects of such redshift binning has recently been examined by Zhu et al. (2016) using mock galaxy catalogues that closely mimic BOSS, and they found their BAO analysis and measurements remained unbiased even when the assumed fiducial cosmology differed from the true (simulation) cosmology. They also confirmed an uncertainty of just 1 per cent on $\alpha^{\rm BAO}$ over a range of different assumptions (fiducial cosmologies, pivot redshifts, redshift-space distortion parameters, and galaxy bias models) which could be further improved to the sub per cent level with future optimal redshift weighting schemes (e.g. Zhu, Padmanabhan & White 2015). For reference, Alam et al. (2017) assumed a 0.3 per cent systematic uncertainty on $\alpha^{\rm BAO}$ from their fitting methodologies.

We note that the redshifts at which the BAO measurements are made are approximate, because they are weighted averages of the redshifts of all of the pairs of galaxies that go into generating the correlation function. The weighting can depend on the choice of using average redshifts or average distances, which adds some uncertainty to the redshift of the distance anchor. However, since

the slope in Fig. 1 is shallow, any uncertainty in the centre of the redshift bin would only add a small uncertainty to the measurement of H_0 (< 0.5 km s^{-1}Mpc^{-1}).

Therefore, the systematic uncertainties on the BAO measurements should be subdominant at present, and should not affect our conclusions given the larger statistical uncertainties on our H_0 results.

4.3 Comparison to Aubourg et al. (2015) and Alam et al. (2017)

In this section, we compare our results to earlier inverse distance ladder measurements by Aubourg et al. (2015) and Alam et al. (2017), using the JLA supernova sample. Aubourg et al. (2015) found $H_0 = 67.3 \pm 1.1$ km s^{-1} Mpc^{-1} with BAOs from BOSS DR11, which changed only marginally to $H_0 = 67.3 \pm 1.0$ km s^{-1} Mpc^{-1} in Alam et al. (2017) with BOSS DR12. We note that these values are consistent with our value of $H_0 = 67.8 \pm 1.3$ Mpc^{-1} using the DES-SN3YR sample, and $H_0 = 67.1 \pm 1.3$ km s^{-1} Mpc^{-1} using JLA.

We emphasize a number of differences in the methods to these papers. Aubourg et al. (2015) and Alam et al. (2017) assumed a model for the redshift–distance relation based on ΛCDM, with the
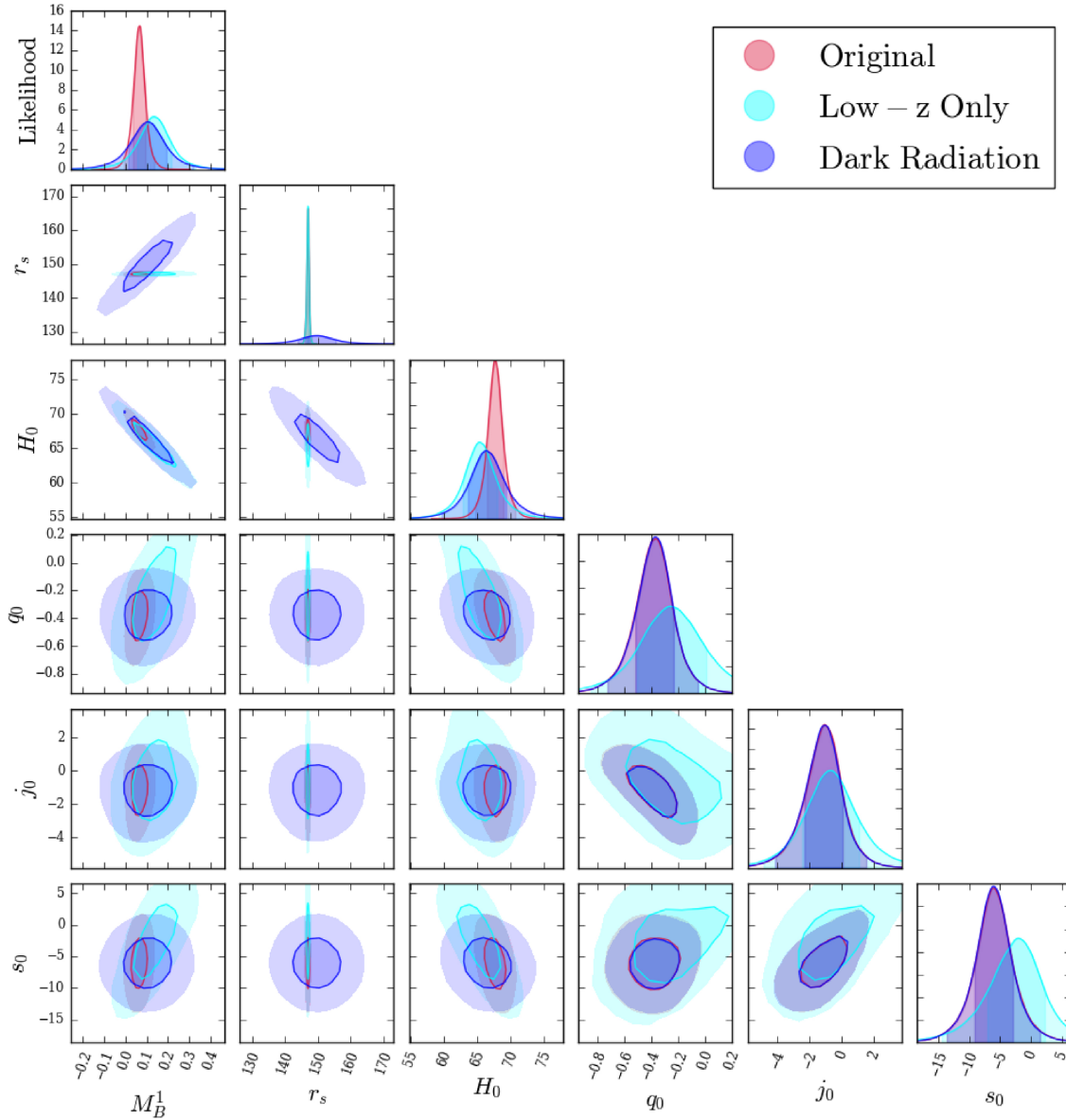
Figure 4. Testing the sensitivity of our parameters to different priors and data cuts. The red contours show our original combined constraints from Fig. 2. In cyan we show the constraints using just the Low-*z* sample, and in blue we show the effect of varying our prior on the sound horizon, to allow for the possibility of early dark radiation.

addition of two additional, arbitrary density components, which scaled to linear and quadratic order with the scale factor, *a*, in order to allow for the possibility of physics beyond ΛCDM. In order to constrain the BAO scale, r_s, these papers applied priors on matter and baryon densities derived from the CMB, and used a fitting function to calculate r_s as a function of these parameters (see Aubourg et al. 2015).

In contrast, our method is more physics agnostic. The cosmographic model we assume means that we do not have to assume a Friedmann model for the redshift–distance relation. The prior on the scale of r_s also means that we are less sensitive to the (albeit, well understood) plasma physics of the CMB.

As for data, we additionally use the BAO measurement from Carter et al. (2018). As illustrated in Fig. 1, we believe that the inclusion of this BAO measurement leads to our marginally lower

value of H_0 with the JLA sample: 67.1, versus 67.3 km s^{-1} Mpc^{-1} in Aubourg et al. (2015) and Alam et al. (2017).

Although our value of H_0 has a larger uncertainty than in Alam et al. (2017; 1.3 versus 1.0 km s^{-1} Mpc^{-1}), this is due to our more physics-agnostic model, as opposed to the data. Comparing both sets of SNe directly with our cosmographic model, we find the same uncertainty with DES-SN3YR as with JLA (1.3 km s^{-1} Mpc^{-1}), even though DES-SN3YR comprises 329 SNe, compared to 740 in JLA.

Moreover, we also include several additional sources of systematic uncertainty which were not included by Betoule et al. (2014). For example, we allow for a systematic uncertainty due to a redshift-shift caused by large-scale inhomogeneities (Calcino & Davis 2017). We also note in Fig. 4 that the uncertainty in the underlying parent population of SNe Ia is one of the dominant

sources of systematic uncertainty (e.g. Guy et al. 2010; Conley et al. 2011).

This smaller uncertainty on H_0 is driven in part by the BBC analysis method (Kessler & Scolnic 2017), and also by the calibration consistency of DECam in the DES SN sample (Flaugher et al. 2015; Brout et al. 2019a). We note, however, that since DES-SN3YR and JLA share some SNe in the Low-z sample, they cannot be combined, as the samples are not entirely independent.

REFERENCES

Addison G. E., Watts D. J., Bennett C. L., Halpern M., Hinshaw G., Weiland J. L., 2018, ApJ, 853, 119
Alam S. et al., 2017, MNRAS, 470, 2617
Anderson L. et al., 2014, MNRAS, 441, 24
Aubourg É. et al., 2015, Phys. Rev. D, 92, 123516
Bassett B. A., Kunz M., 2004, ApJ, 607, 661
Bernal J. L., Verde L., Riess A. G., 2016, J. Cosmol. Astropart. Phys., 10, 019
Betoule M. et al., 2014, A&A, 568, A22
Beutler F. et al., 2011, MNRAS, 416, 3017
Birrer S. et al., 2019, MNRAS, 484, 4726

Blake C., Glazebrook K., 2003, ApJ, 594, 665
Blake C. et al., 2011, MNRAS, 418, 1707
Brout D. et al., 2019a, ApJ, 874, 150
Brout D. et al., 2019b, ApJ, 874, 106
Busca N. G. et al., 2013, A&A, 552, A96
Calcino J., Davis T., 2017, J. Cosmol. Astropart. Phys., 2017, 038
Capozziello S., Cardone V. F., Salzano V., 2008, Phys. Rev. D, 78, 063504
Carter P., Beutler F., Percival W. J., Blake C., Koda J., Ross A. J., 2018, MNRAS, 481, 2371
Conley A. et al., 2011, ApJS, 192, 1
Contreras C. et al., 2010, AJ, 139, 519
Costa A. A., Xu X.-D., Wang B., Abdalla E., 2017, J. Cosmol. Astropart. Phys.., 2017, 028
Croft R. A. C., Dailey M., 2015, Q. Phys. Rev., 1, 1
D'Andrea C. B. et al., 2018, preprint (arXiv:1811.09565)
de Putter R., Linder E. V., Mishra A., 2014, Phys. Rev. D, 89, 103502
DES Collaboration, 2018a, ApJS, 239, 18
DES Collaboration, 2018b, MNRAS, 480, 3879
DES Collaboration, 2018c, preprint (arXiv:1811.02374)
Di Valentino E., Melchiorri A., Silk J., 2016, Phys. Lett. B, 761, 242
Di Valentino E., Melchiorri A., Mena O., 2017, Phys. Rev. D, 96, 043503
Di Valentino E., Linder E. V., Melchiorri A., 2018, Phys. Rev. D, 97, 043528
Eisenstein D. J. et al., 2005, ApJ, 633, 560
Farooq O., Ranjeet Madiyar F., Crandall S., Ratra B., 2017, ApJ, 835, 26
Feeney S. M., Peiris H. V., Williamson A. R., Nissanke S. M., Mortlock D. J., Alsing J., Scolnic D., 2019, Phys. Rev. Lett., 122, 061105
Flaugher B. et al., 2015, AJ, 150, 150
Folatelli G. et al., 2010, AJ, 139, 120
Foreman-Mackey D., Hogg D. W., Lang D., Goodman J., 2013, PASP, 125, 306
Freedman W. L., 2017, Nat. Astron., 1, 0169
Gómez-Valent A., Amendola L., 2018, J. Cosmol. Astropart. Phys., 2018, 051
Grandis S., Rapetti D., Saro A., Mohr J. J., Dietrich J. P., 2016, MNRAS, 463, 1416
Guidorzi C. et al., 2017, ApJ, 851, L36
Guy J. et al., 2007, A&A, 466, 11
Guy J. et al., 2010, A&A, 523, A7
Hamuy M. et al., 2006, PASP, 118, 2
Hicken M. et al., 2009, ApJ, 700, 331
Hicken M. et al., 2012, ApJS, 200, 12
Joudaki S. et al., 2017, MNRAS, 471, 1259
Kelly P. L., Hicken M., Burke D. L., Mandel K. S., Kirshner R. P., 2010, ApJ, 715, 743
Kessler R., Scolnic D., 2017, ApJ, 836, 56
Kessler R. et al., 2009, ApJS, 185, 32
Kessler R. et al., 2019, MNRAS, 485, 1171
Krisciunas K. et al., 2017, AJ, 154, 211
Lampeitl H. et al., 2010a, MNRAS, 401, 2331
Lampeitl H. et al., 2010b, ApJ, 722, 566
Lasker J. et al., 2019, MNRAS, 485, 5329
Le Borgne D., Rocca-Volmerange B., 2002, A&A, 386, 446
Lemos P., Lee E., Efstathiou G., Gratton S., 2019, MNRAS, 483, 4803
Macaulay E., Wehus I. K., Eriksen H. K., 2013, Phys. Rev. Lett., 111, 161301
Moresco M., Verde L., Pozzetti L., Jimenez R., Cimatti A., 2012, J. Cosmol. Astropart. Phys, 7, 053
Muthukrishna D., Parkinson D., 2016, J. Cosmol. Astropart. Phys., 2016, 052
Padmanabhan N., White M., 2008, Phys. Rev. D, 77, 123540
Perlmutter S. et al., 1999, ApJ, 517, 565

Planck Collaboration, 2018, preprint (arXiv:1807.06209)
Pourtsidou A., Tram T., 2016, Phys. Rev. D, 94, 043518
Riess A. G. et al., 1998, AJ, 116, 1009
Riess A. G. et al., 2016, ApJ, 826, 56
Riess A. G. et al., 2018, ApJ, 855, 136
Ross A. J., Samushia L., Howlett C., Percival W. J., Burden A., Manera M., 2015, MNRAS, 449, 835
Scolnic D. et al., 2015, ApJ, 815, 117
Scolnic D. M. et al., 2018, ApJ, 859, 101
Seo H.-J., Eisenstein D. J., 2003, ApJ, 598, 720
Stritzinger M. D. et al., 2011, AJ, 142, 156
Sullivan M. et al., 2010, MNRAS, 406, 782
Vagnozzi S., Giusarma E., Mena O., Freese K., Gerbino M., Ho S., Lattanzi M., 2017, Phys. Rev. D, 96, 123503
Verde L., Bellini E., Pigozzo C., Heavens A. F., Jimenez R., 2017, J. Cosmol. Astropart. Phys., 2017, 023
Wu H.-Y., Huterer D., 2017, MNRAS, 471, 4946
Yang W., Xu L., 2014, Phys. Rev. D, 89, 083517
Yèche C., Palanque-Delabrouille N., Baur J., du Mas des Bourboux H., 2017, J. Cosmol. Astropart. Phys., 2017, 047
Zhang M.-J., Li H., Xia J.-Q., 2017a, Eur. Phys. J. C, 77, 434
Zhang B. R., Childress M. J., Davis T. M., Karpenka N. V., Lidman C., Schmidt B. P., Smith M., 2017b, MNRAS, 471, 2254
Zhao G.-B. et al., 2017, Nat. Astron., 1, 627
Zhu F., Padmanabhan N., White M., 2015, MNRAS, 451, 236
Zhu F., Padmanabhan N., White M., Ross A. J., Zhao G., 2016, MNRAS, 461, 2867

APPENDIX: TESTS OF THE PARAMETER-FITTING CODE

In this section, we test our method with artificially generated SN and BAO distances, to ensure we can recover the input parameters used to generate the distances. To generate the artificial distances, we use our cosmographic model with values chosen at $H_0 = 70.0$ km s^{-1} Mpc^{-1}, $q_0 = -0.55$, $j_0 = -0.85$, $s_0 = -0.9$, $M_B^1 = -19.07$, and $r_s = 147$ Mpc.

To generate the artificial supernova distances, we calculated fiducial distance moduli $\mu^{\rm fid}(z)$ at the redshift values of the genuine supernova data. To generate artificial distance moduli with a realistic dispersion, we drew realizations from a correlated Gaussian distribution centred on $\mu_{\rm fid}$ with covariance given by the genuine data covariance matrix.

We took a similar approach to generating artificial distances for the BOSS DR12 BAO measurements for this cosmographic model. We first calculated a vector of fiducial $H^{\rm fid}(z)$ and $D_m^{\rm fid}(z)$ at the three effective redshift bins of the BAO measurements. To generate realizations of the BAO data, we then drew samples from a correlated Gaussian distribution centred on this observation vector with covariance of the genuine DR12 data covariance matrix.

In total, we generated one hundred artificial realizations of DES-SN3YR and BOSS DR12 data sets. These simulations are shown in Fig. A1 along with the average of these realizations (contours). These simulations confirm we can accurately recover the input parameters, and the uncertainties on the simulated parameter measurements are consistent with our genuine uncertainties.
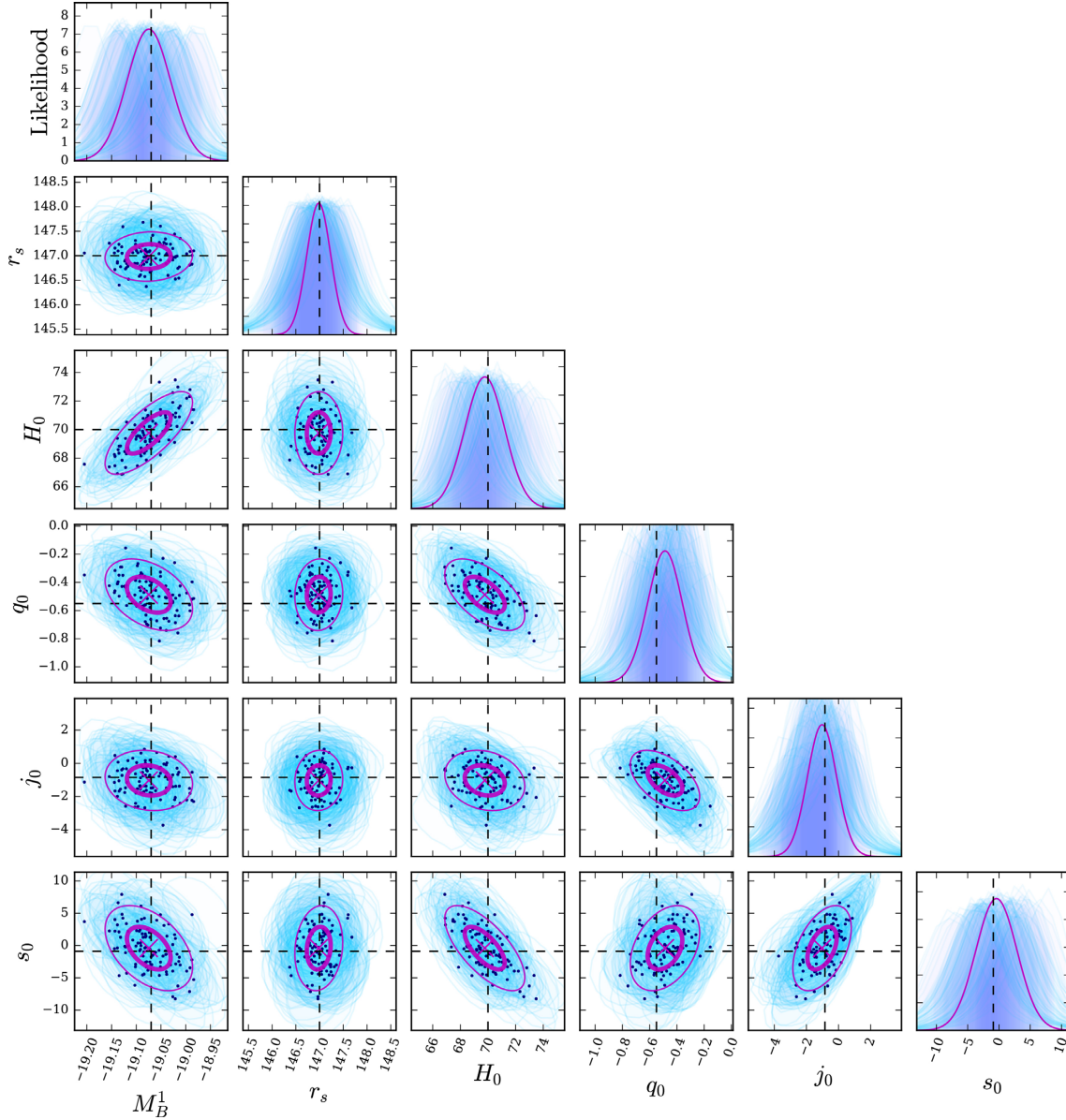
Figure A1. The best-fitting parameters for 100 mock realizations (see text for details). The black dashed lines show the input parameter values for our mock realizations, while the light blue contours show the 68 per cent confidence region for each of the hundred realizations. The dark blue points show the maximum likelihood values for each realization. The magenta ellipses are the one and two standard deviations of these best-fitting points, centred on the magenta crosses, at the averages of the individual maximum likelihood values.

[1]*Institute of Cosmology and Gravitation, University of Portsmouth, Portsmouth PO1 3FX, UK*

[2]*Department of Physics and Astronomy, University of Pennsylvania, Philadelphia, PA 19104, USA*

[3]*School of Mathematics and Physics, University of Queensland, Brisbane, QLD 4072, Australia*

[4]*ARC Centre of Excellence for All-sky Astrophysics (CAASTRO), Australia*

[5]*The Research School of Astronomy and Astrophysics, Australian National University, ACT 2601, Australia*

[6]*African Institute for Mathematical Sciences, 6 Melrose Road, Muizenberg 7945, South Africa*

[7]*South African Astronomical Observatory, P.O.Box 9, Observatory 7935, South Africa*

[8]*Kavli Institute for Cosmological Physics, University of Chicago, Chicago, IL 60637, USA*

[9]*Department of Astronomy and Astrophysics, University of Chicago, Chicago, IL 60637, USA*

[10]*Lawrence Berkeley National Laboratory, 1 Cyclotron Road, Berkeley, CA 94720, USA*

[11]*School of Physics and Astronomy, University of Southampton, Southampton SO17 1BJ, UK*

[12]*Cerro Tololo Inter-American Observatory, National Optical Astronomy Observatory, Casilla 603, La Serena, Chile*

[13]*Fermi National Accelerator Laboratory, P. O. Box 500, Batavia, IL 60510, USA*

[14]*Korea Astronomy and Space Science Institute, Yuseong-gu, Daejeon 305-348, Korea*

[15]*LSST, 933 North Cherry Avenue, Tucson, AZ 85721, USA*

[16]*Department of Physics & Astronomy, University College London, Gower Street, London WC1E 6BT, UK*

[17]*George P. and Cynthia Woods Mitchell Institute for Fundamental Physics and Astronomy, and Department of Physics and Astronomy, Texas A&M University, College Station, TX 77843, USA*

[18]*Kavli Institute for Particle Astrophysics & Cosmology, P. O. Box 2450, Stanford University, Stanford, CA 94305, USA*

[19]*SLAC National Accelerator Laboratory, Menlo Park, CA 94025, USA*

[20]*Centro de Investigaciones Energéticas, Medioambientales y Tecnológicas (CIEMAT), E-28040 Madrid, Spain*

[21]*Laboratório Interinstitucional de e-Astronomia - LIneA, Rua Gal. José Cristino 77, Rio de Janeiro, RJ 20921-400, Brazil*

[22]*INAF, Astrophysical Observatory of Turin, I-10025 Pino Torinese, Italy*

[23]*Department of Astronomy, University of Illinois at Urbana-Champaign, 1002 W. Green Street, Urbana, IL 61801, USA*

[24]*National Center for Supercomputing Applications, 1205 West Clark St, Urbana, IL 61801, USA*

[25]*Institut de Física d'Altes Energies (IFAE), The Barcelona Institute of Science and Technology, Campus UAB, E-08193 Bellaterra (Barcelona), Spain*

[26]*Institut d'Estudis Espacials de Catalunya (IEEC), E-08034 Barcelona, Spain*

[27]*Institute of Space Sciences (ICE, CSIC), Campus UAB, Carrer de Can Magrans, s/n, E-08193 Barcelona, Spain*

[28]*Observatório Nacional, Rua Gal. José Cristino 77, Rio de Janeiro, RJ 20921-400, Brazil*

[29]*Department of Astronomy/Steward Observatory, 933 North Cherry Avenue, Tucson, AZ 85721-0065, USA*

[30]*Jet Propulsion Laboratory, California Institute of Technology, 4800 Oak Grove Dr., Pasadena, CA 91109, USA*

[31]*Department of Astronomy, University of Michigan, Ann Arbor, MI 48109, USA*

[32]*Department of Physics, University of Michigan, Ann Arbor, MI 48109, USA*

[33]*Department of Astronomy, University of California, Berkeley, CA 94720-3411, USA*

[34]*Miller Institute for Basic Research in Science, University of California, Berkeley, CA 94720, USA*

[35]*Santa Cruz Institute for Particle Physics, Santa Cruz, CA 95064, USA*

[36]*PITT PACC, Department of Physics and Astronomy, University of Pittsburgh, Pittsburgh, PA 15260, USA*

[37]*Instituto de Fisica Teorica UAM/CSIC, Universidad Autonoma de Madrid, E-28049 Madrid, Spain*

[38]*Centre for Astrophysics & Supercomputing, Swinburne University of Technology, VIC 3122, Australia*

[39]*CENTRA, Instituto Superior Técnico, Universidade de Lisboa, Av. Rovisco Pais 1, P-1049-001 Lisboa, Portugal*

[40]*Department of Physics, ETH Zurich, Wolfgang-Pauli-Strasse 16, CH-8093 Zurich, Switzerland*

[41]*Center for Cosmology and Astro-Particle Physics, The Ohio State University, Columbus, OH 43210, USA*

[42]*Department of Physics, The Ohio State University, Columbus, OH 43210, USA*

[43]*Max Planck Institute for Extraterrestrial Physics, Giessenbachstrasse, D-85748 Garching, Germany*

[44]*Universitäts-Sternwarte, Fakultät für Physik, Ludwig-Maximilians Universität München, Scheinerstr. 1, D-81679 München, Germany*

[45]*Harvard-Smithsonian Center for Astrophysics, Cambridge, MA 02138, USA*

[46]*Department of Physics, University of Namibia, 340 Mandume Ndemufayo Avenue, Pionierspark, Windhoek 13301, Namibia*

[47]*Australian Astronomical Optics, Macquarie University, North Ryde, NSW 2113, Australia*

[48]*Sydney Institute for Astronomy, School of Physics, A28, The University of Sydney, NSW 2006, Australia*

[49]*Departamento de Física Matemática, Instituto de Física, Universidade de São Paulo, CP 66318 São Paulo, SP 05314-970, Brazil*

[50]*Department of Astronomy, The Ohio State University, Columbus, OH 43210, USA*

[51]*Institució Catalana de Recerca i Estudis Avançats, E-08010 Barcelona, Spain*

[52]*Division of Theoretical Astronomy, National Astronomical Observatory of Japan, 2-21-1 Osawa, Mitaka, Tokyo 181-8588, Japan*

[53]*Institute of Astronomy and Astrophysics, Academia Sinica, Taipei 10617, Taiwan*

[54]*Department of Physics and Astronomy, Pevensey Building, University of Sussex, Brighton BN1 9QH, UK*

[55]*Physics Department, Brandeis University, 415 South Street, Waltham, MA 02453, USA*

[56]*Instituto de Física Gleb Wataghin, Universidade Estadual de Campinas, 13083-859 Campinas, SP, Brazil*

[57]*Computer Science and Mathematics Division, Oak Ridge National Laboratory, Oak Ridge, TN 37831, USA*

[58]*Observatories of the Carnegie Institution for Science, 813 Santa Barbara St, Pasadena, CA 91101, USA*

[59]*Argonne National Laboratory, 9700 South Cass Avenue, Lemont, IL 60439, USA*

This paper has been typeset from a TeX/LaTeX file prepared by the author.